Inorganic Chemistry

Article

pubs.acs.org/IC

"Tail" Tuning of Iron(II) Spin Crossover Temperature by 100 K

Humphrey L. C. Feltham,[†] Chloe Johnson,[‡] Anastasia B. S. Elliott,[†] Keith C. Gordon,[†] Martin Albrecht,[‡] and Sally Brooker*[,†]

[†]Department of Chemistry and the MacDiarmid Institute for Advanced Materials and Nanotechnology, University of Otago, P.O. Box 56, Dunedin 9054, New Zealand

[‡]School of Chemistry & Chemical Biology, University College Dublin, Belfield, Dublin 4, Ireland

Supporting Information

ABSTRACT: Two new **Rdpt** ligands featuring long "tails", **padpt** (*N*-4*H*-1,2,4-triazole-3,5-di(2-pyridyl)palmitamide) and **hpdpt** (4-(4-heptadecafluorooctylphenyl)-3,5-bis(2-pyridyl)-4H-1,2,4-triazole), were made and reacted with $[Fe^{II}(py)_4(NCS)_2]$ to give pinkish-red $[Fe^{II}(\mathbf{padpt})_2(SCN)_2]$ (**1**) and purple-red $[Fe^{II}(\mathbf{hpdpt})_2(SCN)_2]$ (**2**) as solvent-free crystals. Magnetic measurements reveal that both **1** and **2** exhibit complete and reproducible spin crossovers, with a far lower $T_{1/2}$ for the amide-alkyl tailed **1** (182 K) than for the fluorocarbon tailed **2** (248 K), which in turn is far lower than the $T_{1/2}$ of 290 K previously reported for the nonamide-alkyl tailed analogue $[Fe^{II}(\mathbf{C_{16}dpt})_2(SCN)_2]\cdot{}^2/_3H_2O$ (**3**). Structure determinations for **1** and **2** in both the high spin (HS) and low spin (LS) states confirm the expected trans-NCS conformation and reveal that (a) the "tails" interdigitate and (b) the LS forms are less distorted than the HS forms (Σ = 58−70° vs 47−54°). DSC and Raman spectroscopy confirmed the high tail-dependence of the SCO events in **1** and **2**, as well as in **3**, with the Raman data giving $T_{1/2}$ values of 190, 243, and 285 K, respectively. Bright orange single crystals of the solvatomorph $[Fe^{II}(\mathbf{hpdpt})_2(SCN)_2]\cdot MeOH\cdot H_2O$ ($\mathbf{2}_{solv}$) were also structurally and magnetically characterized and, in contrast to **2**, found to remain HS down to 4 K, providing further evidence of the huge impact of crystal packing on SCO. Both **1** and **2** form stable Langmuir films at an air−water interface, a single layer of which can be transferred to a solid support.

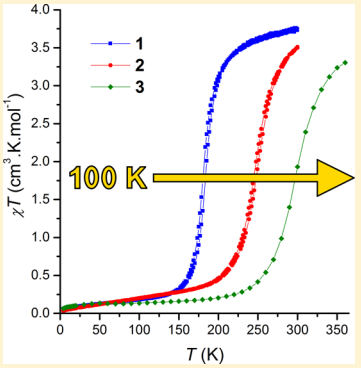

INTRODUCTION

Spin crossover (SCO) occurs in octahedral complexes of d^4 to d^7 metal ions when there is only a small energy difference between the electron pairing energy and the splitting of the t_{2g} and e_g orbitals.[1−3] In such complexes, a small perturbation (usually temperature) can be used to switch between the high-spin (HS) and low-spin (LS) states. This change, HS ↔ LS, is accompanied by changes in the structural, magnetic, and optical properties of the complex, and so SCO active compounds are currently of interest as potential nanosized switches, memory components, sensors, and displays.[2,4,5] Ideally, to be practical as a switch, a complex needs to be able to be immobilized in some fashion such that individual molecules or small groups of molecules can be repeatedly addressed. The self-assembly of amphiphilic complexes into larger, organized structures at an air−water interface, Langmuir−Blodgett (LB) films, and subsequent transfer to a solid support is one way to achieve immobilization of SCO active molecules[6−8] and is the approach taken herein.

The N_6 coordination sphere provided to an iron(II) ion by two 4-substituted bis(2-pyridyl)-4H-1,2,4-triazole (**Rdpt**) ligands and two *trans*-thiocyanate coligands has yielded some nice examples of SCO active compounds.[9] We previously reported that a powder sample (single crystals proved elusive) of an iron(II) complex of an **Rdpt** ligand with a long alkyl tail, $[Fe^{II}(\mathbf{C_{16}dpt})_2(SCN)_2]\cdot{}^2/_3H_2O$ (**3**), exhibits room temperature SCO and forms a stable Langmuir film at an air−water interface.[7] Herein, we demonstrate that modification of the nature of the "tail" allows us to tune the SCO temperature by over 100 K. Specifically, we report and compare the iron(II) complexes of two new types of "tailed" **Rdpt**-based ligands **padpt** and **hpdpt** (Figure 1, amide-alkyl vs phenyl-fluorocarbon tails, i.e. $-N(H)C(=O)C_{15}H_{31}$ vs $-Ph\text{-}p\text{-}C_8F_{17}$ tails), both of which have been structurally characterized in both the LS and HS states, exhibit SCO, form stable films, and can be

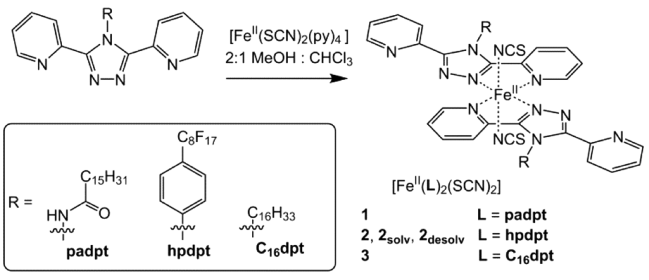

Figure 1. Preparation of $[Fe^{II}(\mathbf{Rdpt})_2(SCN)_2]$ complexes **1** (**Rdpt** = **padpt**), **2**, $\mathbf{2}_{solv}$, and $\mathbf{2}_{desolv}$ (**Rdpt** = **hpdpt**), and previously studied[7] **3** (**Rdpt** = $\mathbf{C_{16}dpt}$).

Received: December 18, 2014
Published: March 2, 2015

DOI: 10.1021/ic503040f
Inorg. Chem. 2015, 54, 2902−2909

transferred to a solid support. The choice of "tail" on the **Rdpt** ligand is shown to exert a dramatic influence on the $T_{1/2}$ of the SCO of the complex, shifting it from 182 (amide-alkyl tail) to 248 (phenyl-fluorocarbon tail) to 290 K (direct link-alkyl tail, i.e. $-C_{16}H_{33}$). Please note that we consider "tail" includes the bond types (amide vs phenyl vs direct connection), tail type (fluorocarbon vs hydrocarbon), and length.

RESULTS AND DISCUSSION

Synthesis. The amide-alkyl-tailed ligand **padpt** was obtained by the condensation of **adpt**[10] with palmitoyl chloride whereas the fluorocarbon-tailed **hpdpt** was obtained by our previously reported general route to **Rdpt** ligands.[11]

Pinkish-red $[Fe^{II}(\mathbf{padpt})_2(SCN)_2]$ (**1**) and purple-red $[Fe^{II}(\mathbf{hpdpt})_2(SCN)_2]$ (**2**) were prepared from the 1:2 reaction of $[Fe^{II}(SCN)_2(py)_4]$[12] with **padpt** or **hpdpt**, respectively (Figure 1), as analytically pure solvent-free crystals (Figure 2 and S5).

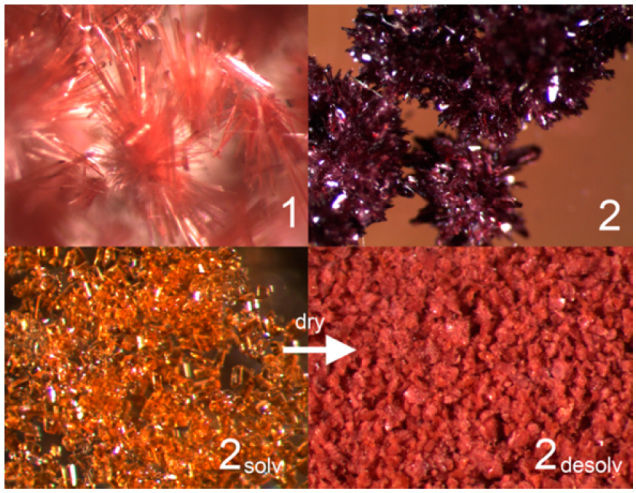

Figure 2. Crystals of solvatomorphs: $[Fe^{II}(\mathbf{padpt})_2(SCN)_2]$ (**1**) is SCO-active; (top right) $[Fe^{II}(\mathbf{hpdpt})_2(SCN)_2]$ (**2**) is SCO-active; (bottom left) $[Fe^{II}(\mathbf{hpdpt})_2(SCN)_2]\cdot MeOH\cdot H_2O$ ($\mathbf{2}_{solv}$) is SCO-inactive; (bottom right) $[Fe^{II}(\mathbf{hpdpt})_2(SCN)_2]$ ($\mathbf{2}_{desolv}$), obtained by drying $\mathbf{2}_{solv}$ under high vacuum for 2 h, is SCO-inactive.

Slow evaporation of the filtrate of **2** gave bright orange crystals of a solvatomorph, $[Fe^{II}(\mathbf{hpdpt})_2(SCN)_2]\cdot MeOH\cdot H_2O$ ($\mathbf{2}_{solv}$) (Figures 1 and 2). The presence of the solvent molecules in $\mathbf{2}_{solv}$ was confirmed by X-ray crystallography, as well as from microanalysis and thermogravometric (TGA) data (Figure S1, ESI). Drying of a sample of orange $\mathbf{2}_{solv}$ at room temperature under high vacuum for 2 h, and air drying overnight, gave a pinkish-red powder sample of $\mathbf{2}_{desolv}$ (Figure 2) that was shown to be solvent-free by elemental analysis and TGA (Figure S1, ESI) but which differs magnetically from **2** (see later). No such polymorphism was observed for **1**.

X-ray Crystallography. X-ray crystal structure determinations on single crystals of **1**, **2**, and $\mathbf{2}_{solv}$ were carried out at 100 and 250 K to investigate the SCO activity of the complexes. This was not possible for $\mathbf{2}_{desolv}$ due to the powder nature of the samples. All three complexes are in the P-1 space group at both temperatures, with the iron(II) center located on a center of inversion and coordinated by two **Rdpt** ligands in the equatorial plane and two thiocyanate anions *trans* to one another in the axial sites (Figures 2−4 and S6−S7, and Tables 1

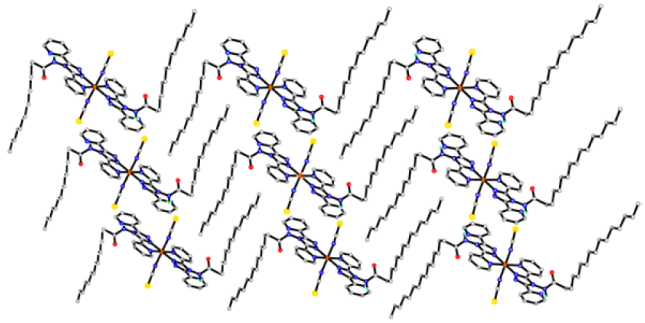

Figure 3. Crystal packing of **1** at 100 K, viewed down the *c*-axis. Only the hydrogen atoms on the amide nitrogen atoms are shown. Color code: gray = carbon, blue = nitrogen, red = oxygen, yellow = sulfur, brown = iron.

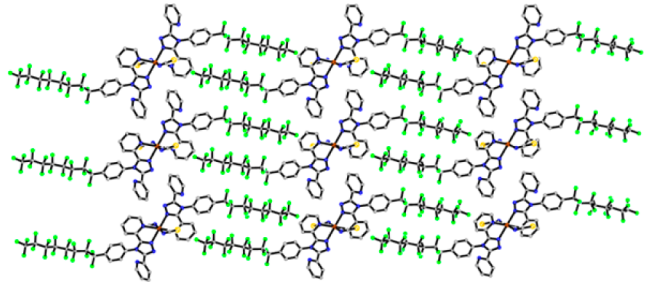

Figure 4. Crystal packing of $\mathbf{2}_{solv}$ at 100 K, viewed down the *b*-axis. For clarity, hydrogen atoms and solvent molecules (Figure S2) have been omitted. Color code as above (Figure 2) plus: shaded green = fluorine.

Table 1. Selected Bond Lengths (Å), and Octahedral Distortion $\sum$ and "Twist" Parameters (deg), for 1, 2, and $\mathbf{2}_{solv}$ at 100 and 250 K

	1		2		$\mathbf{2}_{solv}$	
	100 K	250 K	100 K[a]	250 K[a]	100 K	250 K
$Fe\text{-}_{triaz}$	1.987	2.145	1.95/1.96	2.00/2.07	2.188	2.185
$Fe\text{-}N_{pyr}$	2.022	2.198	2.00/2.00	2.07/2.12	2.196	2.192
$Fe\text{-}_{NCS}$	1.953	2.152	1.93/1.94	1.99/2.05	2.109	2.110
$\sum$	54	70	48/53	59/64	77	77
Twist[b]	83	85	82/89	86/89	74	74

[a]Two unique molecules in the asymmetric unit, and poorer data quality. [b]Twist angle between the triazole ring and the attached NC(=O) or phenyl group.

and S1). The long aliphatic chains of **1** are not quite fully extended due to a kink at the methylene carbon atom adjacent to the amide carbonyl carbon atom, but they are nicely interdigitated with the chains of neighboring molecules (Figure 3). Despite the modest strength of intermolecular C−F···F−C interactions,[13] the C_8F_{17} chains of $\mathbf{2}_{solv}$ are fully extended and interdigitated (Figure 4). Unfortunately, the crystals of **2** diffracted X-rays only weakly, giving low quality data, so the very badly disordered C_8F_{17} chains cannot be resolved. This makes it impossible to comment meaningfully on the packing of the chains in **2**, although from the residual electron density map it appears that the disordered chains are also fairly well extended and interdigitated with those of neighboring molecules.

The Fe^{II}−N bond lengths and octahedral distortion parameters ($\sum$)[14] for **1** and $\mathbf{2}_{solv}$ at 250 K, and for $\mathbf{2}_{solv}$ at 100 K, are consistent with HS iron(II) (Table 1). However, in

DOI: 10.1021/ic503040f
Inorg. Chem. 2015, 54, 2902−2909

the case of **1** at 100 K, these are instead consistent with LS iron(II), so **1** is SCO-active whereas $\mathbf{2}_{solv}$ is SCO inactive over this temperature range. In the case of **2**, all of these parameters are fully consistent with it being LS at 100 K, but at 250 K this compound is mid-SCO ($T_{1/2}$ = 248 K, see later) so the parameters are in-between those expected for HS and for LS (Table 1). As just noted, $\mathbf{2}_{solv}$ is SCO inactive, whereas **2** is SCO active. The solvents present in $\mathbf{2}_{solv}$ are involved in hydrogen bonding and a solvent lone pair−π interaction[15] (Figure S6), whereas there is no solvent in **2**—such differences are well-known to influence spin state (and/or $T_{1/2}$).[16]

In all cases, the twist angle between the triazole ring and the attached amide moiety, N−C(=O), or phenyl ring, lies between 74 and 89° (Table 1). As these are almost perpendicular to one another, there will not be a significant mesomeric interaction between them. Inductive effects are likely to be very modest given the long distances involved. Hence the impact of the tails on the spin crossover is likely to be mostly due to the differences in intermolecular interactions.

Magnetic Susceptibility Studies. Variable-temperature magnetic susceptibility studies were performed on **1**, **2**, $\mathbf{2}_{solv}$, and $\mathbf{2}_{desolv}$ between 300 and 4 K. The magnetic properties of **3** have previously been reported.[7] In the case of **1** and **2**, a range of scan rates was employed to examine the nature of the SCO event in more detail (see Supporting Information (SI)).

At room temperature, the χT products for **1** and **2** are 3.75 and 3.51 $cm^3 \cdot K \cdot mol^{-1}$ (5.48 and 5.30 μ_B), respectively, consistent with both complexes being completely HS (Figure 5). As the temperature is lowered to 30 K, the χT product decreases to 0.10 and 0.08 $cm^3 \cdot K \cdot mol^{-1}$ (0.89 and 0.80 μ_B), respectively, consistent with conversion to the LS state. Upon warming back up to 300 K, the temperature dependence of χT is very similar to that of the cooling mode, but at scan rates ≥1 $K \cdot min^{-1}$ the SCO for **1** and **2** appears to occur with a small (about 3 K wide when scanning at 2 $K \cdot min^{-1}$) thermal hysteresis loop (Figure 5 and S8−S9, SI). However, at higher scan speeds, a narrow loop can simply be due to the temperature of the sample lagging behind that of the instrument thermometer. Hence, the magnetic data on **1** were corrected for this lag, using the previously reported method[17,18] (Figure S3−S4, SI). Unfortunately, it was not possible to correct the magnetic data for **2** for thermal lag (see SI for details). However, given that both the sample masses and the observed loop widths were similar for **1** and **2**, and the loop of **1** closes after correcting for the thermal lag (Figure 6 and S10), the loop of **2** is expected to do the same. When using the sweep mode at slower scan speeds (<1 $K \cdot min^{-1}$), as expected, the lag becomes more-or-less insignificant and there is no thermal hysteresis whether or not a correction is applied.

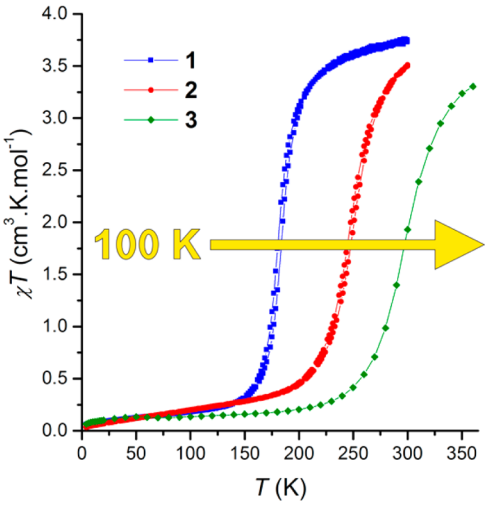

Figure 5. Temperature dependence of the χT product in a **1** kOe dc field of **1** and **2** (data collected in sweep mode at **2** $K \cdot min^{-1}$), along with that previously reported[7] for **3** in a 10 kOe dc field (data collected in settle mode at 5 $K \cdot min^{-1}$), for comparison. Note: Lag corrections have not been applied to the data for **1** or **2** shown in this figure so hysteresis loops are "apparent", but they are not real; rather, this is the result of instrumental limitations (see Figure 6 and SI). Complex **3** does not require a lag correction, as the data for that were collected in settle mode, which does not suffer from this problem, but settle mode is much slower than sweep so it is only possible given ample instrument availability (which is usually limited). The solid lines are not a fit but are simply a guide for the eye.

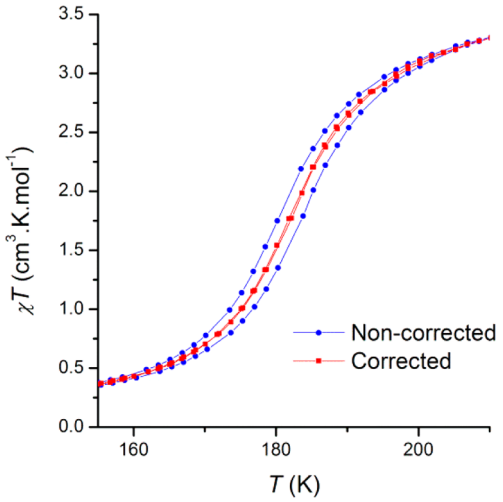

Figure 6. Temperature dependence of the χT product of **1** in a 1000 Oe field between 155 and 210 K, sweeping the temperature at 2 $K \cdot min^{-1}$, with (red squares) or without (blue circles) the data having corrected the lag between the PPMS thermometer and the temperature of the sample (correction results in the "apparent" hysteresis loop closing). The solid lines are simply a guide for the eye. When such a correction is made, it is critically important to present plots of both the noncorrected (raw) and corrected data in the Supporting Information.

In summary, the variable-temperature magnetic data on **1** and **2** show that both undergo reasonably abrupt SCO, with $T_{1/2}$ values of 182 K for **1** (regardless of scan speed after applying the thermal correction) and 248 K for **2** (at scan rates <1 $K \cdot min^{-1}$), though neither complex exhibits SCO with thermal hysteresis.

Variable-temperature magnetic susceptibility studies on $\mathbf{2}_{solv}$ and $\mathbf{2}_{desolv}$ confirmed that the complexes do not undergo SCO down to 4 K (Figure S11). The χT products at 300 K for $\mathbf{2}_{solv}$ and $\mathbf{2}_{desolv}$ are 3.25 and 3.29 $cm^3 \cdot K \cdot mol^{-1}$ (5.10 and 5.13 μ_B), respectively, consistent with both complexes being fully HS. As the temperature is lowered to 30 K, the χT products remain more-or-less the same (3.03 and 3.22 $cm^3 \cdot K \cdot mol^{-1}$) as the value at 300 K, which demonstrates that $\mathbf{2}_{solv}$ and $\mathbf{2}_{desolv}$ are not SCO active.

In contrast to the solvent-free crystals of SCO-active **2**, the methanol and water molecules of crystallization present in the solvatomorph $\mathbf{2}_{solv}$ are stabilizing the HS form and preventing

DOI: 10.1021/ic503040f
Inorg. Chem. 2015, 54, 2902−2909

SCO activity - providing another example of solvent of crystallization being an absolutely critical factor in whether or not SCO behavior is observed.[5,18,19] A difference in packing in the crystal lattices of the pair of true polymorphs, SCO-active **2** and SCO-inactive $\mathbf{2}_{desolv}$, resulting from the different ways they were obtained (the latter by drying crystals of $\mathbf{2}_{solv}$) is the probable cause of the completely different magnetic behavior, but this cannot be readily probed, as $\mathbf{2}_{desolv}$ is a powder.

Differential Scanning Calorimetry Studies. Because SCO is associated with a change in enthalpy, differential scanning calorimetry (DSC) can used to investigate the thermodynamics of the SCO event. DSC data on **1** collected at 5 K min^{-1} (Figure S12−S13, SI) showed $T_{1/2}\downarrow$ = 182 K and $T_{1/2}\uparrow$ = 185 K, which is in excellent agreement with the $T_{1/2}$ values observed directly from the T_{lag}-uncorrected magnetic data collected at 2 K·min^{-1} ($T_{1/2}\downarrow$ = 182 K and $T_{1/2}\uparrow$ = 185 K by PPMS). The data for **2** collected at 5 K min^{-1} (Figure S14−S15, SI) showed $T_{1/2}\downarrow$ = 249 K and $T_{1/2}\uparrow$ = 252 K, which is also in good agreement with the $T_{1/2}$ values determined from magnetic data at 2 K·min^{-1} ($T_{1/2}\downarrow$ = 247 K and $T_{1/2}\uparrow$ = 250 K by PPMS). As with the magnetic data, the small difference in the $T_{1/2}$ values between the cooling and heating modes is likely due to experimental limitations rather than the presence of actual thermal hysteresis.

For **3**, the data showed $T_{1/2}\downarrow = T_{1/2}\uparrow$ = 294 K (Figure S16−S17, SI), which is also in good agreement with the magnetic data ($T_{1/2}\downarrow = T_{1/2}\uparrow$ = 290 K by SQUID in settle mode). The broadness of the peaks in the DSC for the transitions in **3** is consistent with this SCO event being more "gradual", as was observed by magnetic measurements (above).

Integrating the excess heat capacity in the cooling and heating modes for **1**, **2** and **3** (Figure 7 and S12−S17) yields the value of ΔH associated with the transition, and, as $\Delta G = 0$ at $T = T_{1/2}$, this also gives us ΔS for the transition.[20]

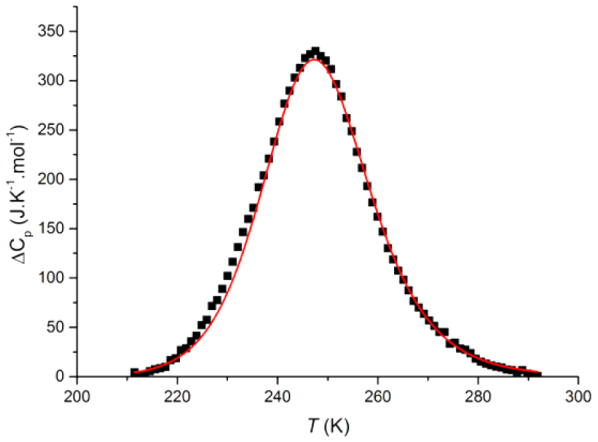

Figure 7. Excess heat capacity (ΔC_p) vs temperature for **2** in the cooling mode (black points). The red line is a Sorai domain model fit (eq 1, below), with $T_{1/2}$ = 248 K and ΔH = 9.1 kJ·mol^{-1}.

The average ΔH and ΔS values for **1**-**3** are in the range ΔH = 7−10 kJ·mol^{-1} and ΔS = 25−47 J·K·mol^{-1} (Table 2). For related iron(II) SCO compounds, ΔH is typically in the range 3−27 kJ·mol^{-1} and ΔS from 22 to 94 J·K·mol^{-1}: [ref21,22] all of the present values fall in these ranges. As expected, the ΔS values associated with the transitions in **1**-**3** are larger than what would be expected purely from the change in electronic structure ($\Delta S_{el} = R \times \mathrm{Ln}((2S_{HS}+1)/(2S_{LS}+1)) = 13$ J·K^{-1}·mol^{-1}), indicating that, as usual, the change in vibrational entropy is a significant contributor to the overall ΔS.[1,21−23]

Table 2. Parameters ΔH (kJ·mol^{-1}), ΔS (J·K·mol^{-1}), and n (Domain Size from the Sorai Model) Obtained from the DSC Data as Described in the Text and SI for 1, 2, and 3

	1	2	3
$\Delta H\downarrow$, $\Delta H\uparrow$ (avg ΔH)	9.4, 8.7 (9)	9.1, 10.6 (10)	8.5, 6.4 (7)
$\Delta S\downarrow$, $\Delta S\uparrow$ (avg ΔS)	51.8, 42.4 (47)	36.9, 42.2 (40)	28.9, 21.8 (25)
$n\downarrow$, $n\uparrow$ (avg n)	6, 9 (8)	8, 6 (7)	8, 12 (10)

Application of the Sorai and Seki Domain Model. With ΔH in hand from the DSC measurements, the Sorai and Seki domain model[20,23,24] can be applied to **1**, **2** and **3** to determine the domain size (n, number of molecules of like spin) associated with the SCO.[18,22,25,26] The larger the value of n, the more cooperative and hence abrupt the SCO is. The value of n is determined by fitting the temperature dependence of the excess heat capacities of the complexes using eq 1:[26]

$$\Delta C_p = \frac{n(\Delta H)^2}{RT^2} \frac{\exp\left[\frac{n\Delta H}{R}\left(\frac{1}{T} - \frac{1}{T_{1/2}}\right)\right]}{\left(1 + \exp\left[\frac{n\Delta H}{R}\left(\frac{1}{T} - \frac{1}{T_{1/2}}\right)\right]\right)^2} \quad (1)$$

where R is the universal gas constant (8.314 J·K^{-1}·mol^{-1}). The average n values for **1**, **2**, and **3** are determined to be 8, 7, and 10 (Table 2, Figure 7, S18−S24, SI). Values of n less than 10, as seen for **1** and **2**, are consistent with small domain sizes and SCO that could be more abrupt (Figure 5).[23] In the case of **3**, where the values of n are slightly higher despite the SCO being observed to be more gradual than in **1** and **2** (Figure 5), the value of n will be less accurate due to the broadness of the peak in the DSC data, which makes determining and modeling the excess heat capacity more difficult. Finally, the agreement between $n\downarrow$ and $n\uparrow$ makes it reasonable to average them, giving n values in the range 7−10, and is also consistent with the absence of thermal hysteresis in these complexes (for hysteretic SCO $n\downarrow \neq n\uparrow$).[20−22]

Raman Spectroscopy Study. Because ligand vibrational modes can be susceptible to the spin state of the metal ion,[1] variable-temperature Fourier-transform Raman spectroscopy can be used to monitor the SCO event. In the case of **1** and **2**, as well as **3**, the C≡N stretch of the thiocyanate anion is a convenient marker as it occurs in an uncluttered region of the Raman spectrum (Figure 8 and Figure S25−S26, SI) and is very sensitive to spin state. The C≡N stretch of the HS and LS forms of **1**, **2** and **3** were readily identified (HS/LS for: **1** 2093/2134; **2** 2064/2111; **3** 2062/2120 cm^{-1}). The intensities of the peaks (calibrated to an internal standard C−H mode at around 2900 cm^{-1}) provide the fraction of HS at each temperature (x) which can be plotted versus T. While less accurate due to the limited number of data points, the $T_{1/2}$ values obtained by fitting a curve to the first derivative of x vs T plot for each of **1**-**3** (Figure S27−S29, SI) are in agreement with those obtained by magnetic measurements (Table 3).

Langmuir−Blodgett Studies. As with **3**,[7] both **1** and **2** spontaneously self-assemble at the air−water interface to form stable Langmuir films. Representative pressure−area isotherms (Figure 9) revealed that densely packed monolayers are accessible, which collapse at a surface areas of between 30 and 40 $Å^2$ per molecule for **1** and **2**. These values are significantly smaller than the calculated area of unfunctionalized

DOI: 10.1021/ic503040f
Inorg. Chem. 2015, 54, 2902−2909

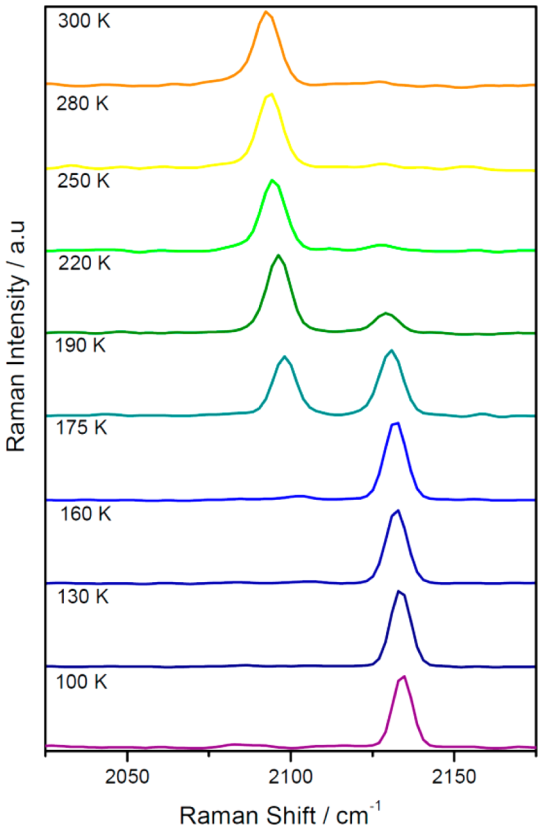

Figure 8. Monitoring the iron(II) spin state in **1** by using Raman spectroscopy to probe the C≡N stretch of the thiocyanate ion (between 2000 and 2200 cm^{-1}) as a function of temperature (100–300 K). The data were collected in cooling mode at a sweep rate of approximately 0.4 $K \cdot min^{-1}$. Excitation wavelength 1064 nm.

Table 3. Summary of the $T_{1/2}$ (K) Values Determined from the Magnetic, DSC, and Raman Data for 1, 2, and 3

	1	2	3
Magnetic data	182[a]	248[a]	290[b,7]
DSC data[c] at 5 $K \cdot min^{-1}$	183	249	295
Raman data[d]	190	243	285

[a]At 0.5 $K \cdot min^{-1}$. [b]In settle mode. [c]For DSC data obtained at 5 $K \cdot min^{-1}$, there is a slight discrepancy between $T_{1/2}\downarrow$ and $T_{1/2}\uparrow$ (see text) similar to when the PPMS sweep rate is high, which is likely due to instrumental limitations rather than actual thermal hysteresis, so the average value is presented here. [d]The $T_{1/2}$ values obtained from analysis of the Raman spectra are less accurate due to the limited number of data points (see Figures S27–S29, SI).

$[Fe^{II}(\mathbf{dpt})_2(SCN)_2]$ (63 Å^2),[7] which suggests that the portion of the molecule orientated toward the hydrophilic surface is not lying completely flat. The area per molecule at the film collapse is also smaller than when using $[Fe^{II}(\mathbf{C_{16}dpt})_2(SCN)_2]\cdot{}^2/_3H_2O$ (~60 A^2),[7] which may be due to a different mode of assembly. Pleasingly, the *monolayers formed are stable over prolonged periods*, as indicated by the absence of a surface pressure decrease when keeping the Langmuir monolayer at a constant barrier position (Figure 9). The stability over time indicates that the lower-than-expected area per molecule values are not due to some of the complexes dissociating in the water layer, as was observed previously with the related complexes $[Fe^{II}(\mathbf{adpt})_2(C_{16}SO_3)_2]$ and $[Fe^{II}(\mathbf{pldpt})_2(C_{16}SO_3)_2]$, which

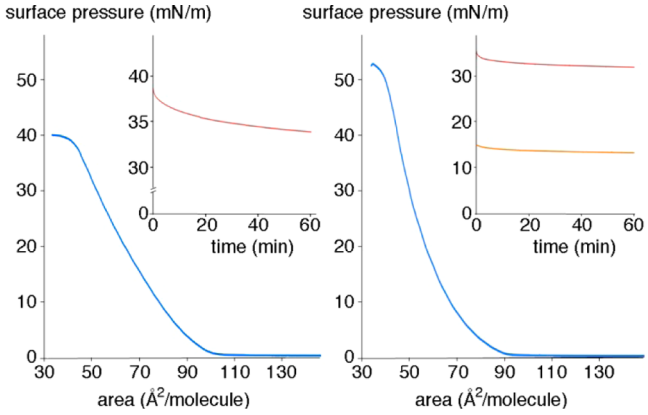

Figure 9. Pressure area isotherms and stability plots (insets) for: (left) **1**, stability plot at 37 $mN \cdot m^{-1}$; (right) **2**, stability plots at 15 (orange line) and 35 $mN \cdot m^{-1}$ (red line).

featured "tailed" anions[8] rather than "tailed" **Rdpt** ligands as in the present complexes.

Transfer of the Langmuir films onto a glass support proceeded with a close to ideal transfer ratio in the first upstroke (Table S1, SI). But in the subsequent downstroke, to place a second layer of complex molecules on top of the first layer, the first layer was quantitatively desorbed onto the air–water interface again, suggesting only moderate adhesion of the complex to the support. Unfortunately, with only one layer of complex absorbed on the surface the spin state cannot be observed by the methods available to us (XMCD is not readily available).

CONCLUSION

We have prepared two new "tailed" iron(II) complexes, **1** and **2**, of formula $[Fe^{II}(\mathbf{Rdpt})_2(SCN)_2]$. Both complexes have been structurally characterized in both spin states (although it should be noted that **2** is clearly not fully HS at 250 K) and further probed by variable-temperature magnetic and Raman studies as well as DSC measurements. These show that they undergo complete and reasonably abrupt SCO and demonstrate remarkable tuning of $T_{1/2}$, by over 100 K, by choice of ligand "tail", from 182 K in amide-alkyl tailed **1** ($-N(H)C(=O)C_{15}H_{31}$ tail), to 248 K for fluorocarbon tailed **2** ($-Ph\text{-}p\text{-}C_8F_{17}$ tail), to being centered around room temperature (290 K) in the nonamide-alkyl tailed **3** ($-C_{16}H_{33}$ tail).

In addition, we clearly demonstrate that a solvatomorph of **2** with interstitial methanol and water molecules, $\mathbf{2}_{solv}$, is SCO inactive, further reinforcing the importance of changes in the packing interactions brought about by what otherwise appear to be relatively minor changes in composition. Furthermore, drying of $\mathbf{2}_{solv}$ generates a true polymorph of SCO-active **2**, $\mathbf{2}_{desolv}$ (neither contain any solvent), which is SCO-inactive.

For the benefit of newcomers to magnetic data collection: while "settle" mode is the gold standard, it is recognized that on high demand instruments (operating under considerable time pressures) it may be necessary to use the faster "sweep" mode. We clearly demonstrate herein that in such cases the sweep rate must be reported and consideration given to whether a T_{lag} correction is required: neither of the present SCO-active complexes exhibited thermal hysteresis once a correction for the lag between the thermometer and the sample temperature was applied (in which case both the raw and corrected data should be supplied in the Supporting Information).

DOI: 10.1021/ic503040f
Inorg. Chem. 2015, 54, 2902–2909

Both **1** and **2** form stable monolayers at an air−water interface (as does **3**[7]), showing that the film-forming ability of the complex has been retained despite the significant changes to the tail. However, although one layer of these films can be transferred onto a glass solid support, multilayers could not be achieved for either complex. As multilayers are desirable, attempts to use other solid supports, and work to prepare complexes of ligands with different types of "tails" that should facilitate the formation of stable multilayers on a solid support, are underway.

EXPERIMENTAL SECTION

A summary of single crystal structure parameters for **1**, **2** and $\mathbf{2}_{solv}$ at both 100 and 250 K is provided in Table S2.

All instrumentation details are provided in the Supporting Information.

***N*-4*H*-1,2,4-triazole-3,5-di(2-pyridyl)palmitamide (padpt).** Under argon, K_2CO_3 (0.35 g, 2.5 mmol) was suspended in a solution of **adpt**[10] (0.5 g, 2.1 mmol) and palmitoyl chloride (0.576 g, 2.1 mmol) in dry $CHCl_3$ (10 mL), and the mixture stirred for 4 h, then filtered. The filtrate was taken to dryness, giving an off-white solid that was recrystallized from hot EtOH. The resulting solid was washed with cold MeCN (2 × 5 mL) and dried in air, yielding **padpt** as a white powder (0.555 g, 56%). Found: C, 70.60; H, 8.52; N, 17.56. Calculated for $C_{28}H_{40}N_6O$: C, 70.55; H, 8.46; N, 17.63; Cl, 0.00. ^{1}H NMR ($CDCl_3$, 400 MHz): 10.28 (s, N*H*); 8.65 (m, 2H, py-*H*), 8.29 (d, *J* = 7.9 Hz, 2H, py-*H*); 7.91 (td, *J* = 7.9, 7.8, 1.7 Hz, 2H, py-*H*); 7.42 (ddd, *J* = 7.7, 5.0, 1.2 Hz, 2H, py-*H*); 2.30 (t, *J* = 7.5, 2H, -C(=O)-C**H**$_2$-); 1.59 (m, 2H, −CO−CH$_2$−C**H**$_2$-), 1.25−1.20 (m, 24H, −CO−CH$_2$−CH$_2$−(C**H**$_2$)$_{12}$-CH$_3$); 0.88 (m, 3H, CH$_3$).

***N*-(4-heptadecafluoroctylphenyl)-2-pyridinethiocarbamide.** 4-Heptadecafluor-octylaniline (1 g, 1.9 mmol), sulfur (0.188 g, 5.9 mmol) and sodium sulfide nonhydrate (0.01 g, 0.04 mmol) were refluxed in 2-methylpyridine (30 mL) for 72 h, after which time the solution was cooled and taken to dryness. The resulting brown solid was suspended in water (80 mL) and the suspension extracted with DCM (3 × 75 mL). The organic fractions were combined, washed with water (100 mL), dried over $MgSO_4$, then reduced in volume to ∼50 mL before being loaded onto a silica gel column. Eluting with chloroform gave the product (R_f = 0.95) as an orange solid (3 g, 100%). Calculated for $C_{20}H_9N_2S_2F_{17}$: C, 37.99; H, 1.41; N, 4.43; S, 5.07. Found: C, 38.11; H, 1.41; N, 4.45; S, 5.17. ^{1}H NMR ($CDCl_3$, 400 MHz) 12.81 (s, 1H, NH), 8.79 (dt, *J* = 8.1, 1.0, 1.0 Hz, 1H, py-H), 8.54 (ddt, *J* = 4.7, 1.7, 0.9 Hz, 1H, py-H), 8.34 (d, *J* = 8.6 Hz, 2H, Ph-H), 7.93 (ddd, *J* = 8.0, 7.5, 1.7 Hz, 1H, py-H), 7.68 (d, *J* = 8.6 Hz, 2H, Ph-H), 7.52 (ddd, *J* = 7.5, 4.7, 1.2 Hz, 1H, py-H). Please note that fluorine analysis can be inaccurate when the percentage fluorine is high.

Ethyl *N*-(heptadecafluoroctylphenyl)pyridine-2-carboimidothioate. Sodium (0.08 g, 3.6 mmol) was reacted with freshly distilled EtOH (75 mL), then *N*-(4-iodophenyl)-2-pyridinethiocarbamide (2.276 g, 3.6 mmol) and bromoethane (0.27 mL, 0.392 3.6 mmol) were added and the resulting solution heated at 50 °C for 4 h, during which time some white sodium bromide precipitated. The suspension was taken to dryness and the resulting solid suspended in DCM (100 mL), the salt filtered off and the filtrate washed with water (3 × 50 mL), saturated aqueous sodium carbonate (50 mL) then saturated aqueous sodium chloride (50 mL). The organic fraction was dried with $MgSO_4$, then taken to dryness yielding crude ethyl *N*-(4-iodophenyl)-pyridine-2-carboimidothioate as an orange oil. This oil was used in the subsequent reaction without any further purification. ^{1}H NMR ($CDCl_3$, 400 MHz) 8.65 (m, 1H, py-H), 8.51 (dt, J = 5.0, 1.5, 1.5 Hz, 1H, py-H), 7.59 (td, J = 7.8, 7.8, 1.7 Hz, 2H, py-H), 7.46 (m, 1H, py-H), 8.3 (m, 1H, Ph-H), 6.87 (d, J = 8.3 Hz, 2H, Ph-H), 4.49 (q, J = 7.1 Hz, 2H, CH_2), 1.48 (t, J = 7.1 Hz, 3H, CH_3).

4-(4-Heptadecafluoroctylphenyl)-3,5-bis(2-pyridyl)-4*H*-1,2,4-triazole (hpdpt). To crude ethyl *N*-(4-heptadecafluoroctylphenyl)pyridine-2-carboimidothioate (2.217 g, 3.3 mmol) in ^{n}BuOH (30 mL) was suspended pyridine-2-carbohydrazide (0.550 g, 4.0 mmol) and the reaction stirred at reflux for 22 h. The solution was cooled to room temperature then further in the fridge, resulting in the precipitation of white solid. The solid was filtered and washed with cold ^{n}BuOH (3 × 10 mL) to afford **hpdpt** (0.549, 23%) as white powder. Found: C, 43.69; H, 1.71; N, 9.64. Calculated for $C_{26}H_{12}N_5F_{17}$: C, 43.53; H, 1.69; N, 9.76. ^{1}H NMR ($CDCl_3$, 400 MHz). 8.22 (m, 4H, 2 × py-H), 7.78 (td, J = 7.8, 7.8, 1.8 Hz, 2H, py-H), 7.59 (d, J = 8.3 Hz, 2H, Ph-H), 7.41 (d, J = 8.3 Hz, 2H, Ph-H), 7.22 (ddd, J = 7.8, 4.8, 1.2, 2H, py-H).

[Fe^{II}(padpt)$_2$(SCN)$_2$] (1). To a solution of **padpt** (0.1 g, 0.21 mmol) in MeOH:$CHCl_3$ (1:1, 6 mL) was added [Fe^{II}(SCN)$_2$(py)$_4$][12] (0.051 g, 0.1 mmol) in MeOH (3 mL) dropwise, and the resulting red solution stirred for 1 h. Diffusion of diethyl ether vapor into the reaction solution yielded red crystals which were filtered, washed with cold MeOH (3 × 2 mL) and dried in air giving **1** (0.052 g, 44%). Found: C, 62.05; H, 7.40; N, 17.67; S, 5.64. Calculated for $FeC_{58}H_{80}N_{14}O_2S_2$: C, 61.91; H, 7.17; N, 17.43; S, 5.70.

[Fe^{II}(hpdpt)$_2$(SCN)$_2$] (2). Onto a solution of **hpdpt** (0.1 g, 0.14 mmol) in $CHCl_3$ (3 mL) was carefully layered MeOH (3 mL). Onto this was carefully further layered a solution of [Fe^{II}(py)$_4$(SCN)$_2$] (0.034 g, 0.07 mmol) in MeOH (3 mL). After 1 week, the resulting dark purple crystals were filtered, washed with cold MeOH (3 × 2 mL) and dried in air giving solvent-free **2** (0.024 g, 25%). Found: C, 40.35; H, 1.57; N, 10.42; S, 3.84; F, 40.44. Calculated for $C_{54}H_{24}N_{12}F_{34}S_2Fe$: C, 40.37; H, 1.51; N, 10.46; S, 3.99; F, 40.20.

[Fe^{II}(hpdpt)$_2$(SCN)$_2$]·MeOH·H$_2$O ($\mathbf{2}_{solv}$). After filtering off **2** as described above, slow evaporation of the filtrate gave a small amount of orange crystals which were filtered and air-dried, yielding the solvatomorph $\mathbf{2}_{solv}$ (0.06 g, 5%). Found: C, 39.95; H, 1.87; N, 10.04; S, 3.87. Calculated for $C_{55}H_{30}N_{12}F_{34}S_2O_2Fe$: C, 39.87; H, 1.83; N, 10.14; S, 3.87.

[Fe^{II}(hpdpt)$_2$(SCN)$_2$] ($\mathbf{2}_{desolv}$). A 0.08 g sample of $\mathbf{2}_{solv}$ was dried under high vacuum at room temperature for 2 h, then left to air-dry overnight at room temperature, yielding the solvent-free solvatomorph $\mathbf{2}_{desolv}$ as pinkish-red powder. Found: C, 40.23; H, 1.54; N, 10.29; S, 3.85. Calculated for $C_{54}H_{24}N_{12}F_{34}S_2Fe$: C, 40.37; H, 1.51; N, 10.46; S, 3.99. TGA: found 3.0% weight loss vs calculated 3.8% for loss of 1 x MeOH and 1 x H_2O.

The synthesis of **C$_{16}$dpt** and [Fe^{II}(**C$_{16}$dpt**)$_2$(SCN)$_2$] has been described previously.[7]

ASSOCIATED CONTENT

Supporting Information

Details of reagents and instruments used; TGA results; photos of samples of $\mathbf{2}_{solv}$ and $\mathbf{2}_{desolv}$; details of T_{lag} corrections, Langmuir transfer ratios and X-ray crystallography; additional figures of variable-temperature magnetism, Raman and DSC data, Sorai modeling, and the structures and packing of the complexes (CCDC 1032519−1032524). This material is available free of charge via the Internet at http://pubs.acs.org.

AUTHOR INFORMATION

Corresponding Author

* E-mail: sbrooker@chemistry.otago.ac.nz. Phone: 64-3-479-7919.

Notes

The authors declare no competing financial interests.

ACKNOWLEDGMENTS

This work was supported by the MacDiarmid Institute for Advanced Materials and Nanotechnology and the Marsden Fund (postdoctoral fellowships to H.L.C.F.), the Irish Research Council (fellowship to C.J.), and the ERC. We also thank Dr. Shen Chong (Robinson Research Institute) for his assistance with operation of the PPMS and SQUID instruments, and Dr.

DOI: 10.1021/ic503040f
Inorg. Chem. 2015, 54, 2902−2909

J. L. Tallon (Robinson Research Institute) for his help and advice.

REFERENCES

(1) Gütlich, P.; Goodwin, H. A. *Top. Curr. Chem.* **2004**, *233*, 1−47.
(2) Gütlich, P.; Gaspar, A. B.; Garcia, Y. *Beilstein J. Org. Chem.* **2013**, *9*, 342−391.
(3) Halcrow, M. A. *Spin-Crossover Materials: Properties and Applications*, 1st ed.; John Wiley & Sons, Ltd: 2013.
(4) (a) Gaspar, A. B.; Seredyuk, M. *Coord. Chem. Rev.* **2014**, *268*, 41−58. (b) Sy, M.; Varret, F.; Boukheddaden, K.; Bouchez, G.; Marrot, J.; Kawata, S.; Kaizaki, S. *Angew. Chem., Int. Ed.* **2014**, *53*, 7539−7542. (c) Coronado, E.; Minguez Espallargas, G. *Chem. Soc. Rev.* **2013**, *42*, 1525−1539. (d) Shepherd, H. J.; Gural'skiy, I. A.; Quintero, C. M.; Tricard, S.; Salmon, L.; Molnár, G.; Bousseksou, A. *Nature Commun.* **2013**, *4*, 2607. (e) Schafer, B.; Rajnak, C.; Salitros, I.; Fuhr, O.; Klar, D.; Schmitz-Antoniak, C.; Weschke, E.; Wende, H.; Ruben, M. *Chem. Commun.* **2013**, *49*, 10986−10988. (f) Roubeau, O. *Chem.—Eur. J.* **2012**, *18*, 15230−15244. (g) Cavallini, M.; Bergenti, I.; Milita, S.; Kengne, J. C.; Gentili, D.; Ruani, G.; Salitros, I.; Meded, V.; Ruben, M. *Langmuir* **2011**, *27*, 4076−4081. (h) Raza, Y.; Volatron, F.; Moldovan, S.; Ersen, O.; Huc, V.; Martini, C.; Brisset, F.; Gloter, A.; Stephan, O.; Bousseksou, A.; Catala, L.; Mallah, T. *Chem. Commun.* **2011**, *47*, 11501−11503. (i) Halcrow, M. A. *Chem. Soc. Rev.* **2011**, *40*, 4119−4142. Bousseksou, A.; Molnár, G.; Salmon, L.; Nicolazzi, W. *Chem. Soc. Rev.* **2011**, *40*, 3313−3335. (j) Cobo, S.; Molnár, G.; Real, J. A.; Bousseksou, A. *Angew. Chem., Int. Ed.* **2006**, *45*, 5786−5789. (k) Murray, K. S.; Kepert, C. J. *Top. Curr. Chem.* **2004**, *233*, 195−228. (l) Létard, J.-F.; Guionneau, P.; Goux-Capes, L. *Top. Curr. Chem.* **2004**, *234*, 221−250.
(5) Muñoz-Lara, F. J.; Gaspar, A. B.; Muñoz, M. C.; Lysenko, A. B.; Domasevitch, K. V.; Real, J. A. *Inorg. Chem.* **2012**, *51*, 13078−13080.
(6) (a) Cavallini, M. *Phys. Chem. Chem. Phys.* **2012**, *14*, 11867−11876. (b) Gandolfi, C.; Cotting, T.; Martinho, P. N.; Sereda, O.; Neels, A.; Morgan, G. G.; Albrecht, M. *Dalton Trans.* **2011**, *40*, 1855−1865. (c) Roubeau, O.; Natividad, E.; Agricole, B.; Ravaine, S. *Langmuir* **2007**, *23*, 3110−3117. (d) Roubeau, O.; Agricole, B.; Clérac, R.; Ravaine, S. *J. Phys. Chem. B* **2004**, *108*, 15110−15116. (e) Sharma, S.; Radhakrishnan, T. P. *J. Phys. Chem. B* **2003**, *107*, 147−156. (f) Soyer, H.; Dupart, E.; Mingotaud, C.; Gomez-Garcia, C.; Delhaes, P. *Colloids Surf., A* **2000**, *171*, 275−282. (g) Soyer, H.; Dupart, E.; Gómez-García, C. J.; Mingotaud, C.; Delhaès, P. *Adv. Mater.* **1999**, *11*, 382−384. (h) Létard, J. F.; Nguyen, O.; Soyer, H.; Mingotaud, C.; Delhaes, P.; Kahn, O. *Inorg. Chem.* **1999**, *38*, 3020−3021. (i) Boillot, M.-L.; Sour, A.; Delhae, P.; Mingotaud, C.; Soyer, H. *Coord. Chem. Rev.* **1999**, *190−192*, 47−59. (j) Soyer, H.; Mingotaud, C.; Boillot, M.-L.; Delhaes, P. *Langmuir* **1998**, *14*, 5890−5895. (k) Soyer, H.; Mingotaud, C.; Boillot, M.-L.; Delhaes, P. *Thin Solid Films* **1998**, *327−329*, 435−438. (l) Kahn, O.; Armand, F.; Badoux, C.; Bonville, P.; Ruaudel-Teixier, A. *Langmuir* **1995**, *11*, 3467−3472. (m) Coronel, P.; Ruaudel-Teixier, A.; Barraud, A. K. O. *Mater. Res. Soc. Symp. Proc.* **1990**, *173*, 537−541. (n) Coronel, P.; Barraud, A.; Claude, R.; Kahn, O.; Ruadel-Teixier, A.; Zarembowitch, J. *J. Chem. Soc., Chem. Commun.* **1989**, 193−194. (o) Ruaudel-Teixier, A.; Barrauda, A.; Coronela, P.; Kahn, O. *Thin Solid Films* **1988**, *160*, 107−115.
(7) Kitchen, J. A.; White, N. G.; Gandolfi, C.; Albrecht, M.; Jameson, G. N. L.; Tallon, J. L.; Brooker, S. *Chem. Commun.* **2010**, *46*, 6464−6466.
(8) White, N. G.; Feltham, H. L. C.; Gandolfi, C.; Albrecht, M.; Brooker, S. *Dalton Trans.* **2010**, *39*, 3751−3758.
(9) Aromí, G.; Barrios, L. A.; Roubeau, O.; Gamez, P. *Coord. Chem. Rev.* **2011**, *255*, 485−546. Kitchen, J. A.; Brooker, S. *Coord. Chem. Rev.* **2008**, *252*, 2072−2092.
(10) (a) Mandal, S. K.; Clase, H. J.; Bridson, J. N.; Ray, S. *Inorg. Chim. Acta* **1993**, *209*, 1−4. (b) Geldard, J. F.; Lions, F. *J. Org. Chem.* **1965**, *30*, 318−319.
(11) Klingele, M. H.; Brooker, S. *Eur. J. Org. Chem.* **2004**, 3422−3434.
(12) Tao, J.-Q.; Gu, Z.-G.; Wang, T.-W.; Yang, Q.-F.; Zuo, J.-L.; You, X.-Z. *Inorg. Chim. Acta* **2007**, *360*, 4125−4132.
(13) Baker, R. J.; Colavita, P. E.; Murphy, D. M.; Platts, J. A.; Wallis, J. D. *J. Phys. Chem. A* **2012**, *116*, 1435−1444.
(14) (a) Guionneau, P.; Brigouleix, C.; Barrans, Y.; Goeta, A. E.; Létard, J.-F.; Howard, J. A. K.; Gaultier, J.; Chasseau, D. *Comptes Rendus Acad. Sci. Ser. IIc* **2001**, *4*, 161−171. (b) Deeney, F. A.; Charles, J. H.; Morgan, G. G.; McKee, V.; Nelson, J.; Teat, S. J.; Clegg, W. *J. Chem. Soc., Dalton Trans.* **1998**, 1837−1843. (c) Drew, M. G. B.; Harding, C. J.; McKee, V.; Morgan, G. G.; Nelson, J. *J. Chem. Soc., Chem. Commun.* **1995**, 1035−1038.
(15) White, N. G.; Kitchen, J. A.; Brooker, S. *Eur. J. Inorg. Chem.* **2009**, 1172−1180. Mooibroek, T. J.; Gamez, P.; Reedijk, J. *CrystEngComm* **2008**, *10*, 1501−1515.
(16) (a) Lochenie, C.; Bauer, W.; Railliet, A. P.; Schlamp, S.; Garcia, Y.; Weber, B. *Inorg. Chem.* **2014**, *53*, 11563−11572. (b) Weber, B.; Bauer, W.; Pfaffeneder, T.; Dîrtu, M. M.; Naik, A. D.; Rotaru, A.; Garcia, Y. *Eur. J. Inorg. Chem.* **2011**, 3193−3206.
(17) Miller, R. G.; Narayanaswamy, S.; Tallon, J. L.; Brooker, S. *New J. Chem.* **2014**, *38*, 1932−1941. Hogue, R. W.; Miller, R. M.; White, N. G.; Feltham, H. L. C.; Jameson, G. N. L.; Brooker, S. *Chem. Commun.* **2014**, *50*, 1435−1437.
(18) Kulmaczewski, R.; Olguín, J.; Kitchen, J. A.; Feltham, H. L. C.; Jameson, G. N. L.; Tallon, J. L.; Brooker, S. *J. Am. Chem. Soc.* **2014**, *136*, 878−881.
(19) (a) Wiedemann, D.; Grohmann, A. *Dalton Trans.* **2014**, *43*, 2406−2417. (b) Clemente-León, M.; Coronado, E.; López-Jordà, M.; Waerenborgh, J. C.; Desplanches, C.; Wang, H.; Létard, J.-F.; Hauser, A.; Tissot, A. *J. Am. Chem. Soc.* **2013**, *135*, 8655−8667. (c) Harding, D. J.; Phonsri, W.; Harding, P.; Gass, I.; Murray, K. S.; Moubaraki, B.; Cashion, J. D.; Liu, L.; Telfer, S. *Chem. Commun.* **2013**, 6340−6342. (d) Harding, D. J.; Sertphon, D.; Harding, P.; Murray, K. S.; Moubaraki, B.; Cashion, J. D.; Adams, H. *Chem.—Eur. J.* **2013**, *19*, 1082−1090. (e) Chen, X.-Y.; Shi, H.-Y.; Huang, R.-B.; Zheng, L.-S.; Tao, J. *Chem. Commun.* **2013**, *49*, 10977−10979. (f) Craig, G. A.; Costa, J. S.; Roubeau, O.; Teat, S. J.; Aromí, G. *Eur. J. Inorg. Chem.* **2013**, 745−752. (g) Chuang, Y.-C.; Liu, C.-T.; Sheu, C.-F.; Ho, W.-L.; Lee, G.-H.; Wang, C.-C.; Wang, Y. *Inorg. Chem.* **2012**, *51*, 4663−4671. (h) Hasegawa, Y.; Sakamoto, R.; Takahashi, K.; Nishihara, H. *Inorg. Chem.* **2013**, *52*, 1658−1665. (i) Ross, T. M.; Moubaraki, B.; Turner, D. R.; Halder, G. J.; Chastanet, G.; Neville, S. M.; Cashion, J. D.; Létard, J.-F.; Batten, S. R.; Murray, K. S. *Eur. J. Inorg. Chem.* **2011**, 1395−417. (j) Li, B.; Wei, R.-J.; Tao, J.; Huang, R.-B.; Zheng, L.-S.; Zheng, Z. *J. Am. Chem. Soc.* **2010**, *132*, 1558−1566. (k) Jameson, G. N. L.; Werner, F.; Bartel, M.; Absmeier, A.; Reissner, M.; Kitchen, J. A.; Brooker, S.; Caneschi, A.; Carbonera, C.; Létard, J.-F.; Linert, W. *Eur. J. Inorg. Chem.* **2009**, *26*, 3948−3959.
(20) Kahn, O. *Molecular Magnetism*; VCH Publishers Inc.: New York, 1993.
(21) Roubeau, O.; Castro, M.; Burriel, R.; Haasnoot, J. G.; Reedijk, J. *J. Phys. Chem. B* **2011**, *115*, 3003−3012.
(22) Arcis-Castíllo, Z.; Zheng, S.; Siegler, M. A.; Roubeau, O.; Bedoui, S.; Bonnet, S. *Chem.—Eur. J.* **2011**, *17*, 14826−14836.
(23) Sorai, M. *Top. Curr. Chem.* **2004**, *235*, 153−170.
(24) Sorai, M.; Seki, S. *J. Phys. Chem. Solids* **1974**, *35*, 555−570.
(25) (a) Wannarit, N.; Nassirinia, N.; Amani, S.; Masciocchi, N.; Youngme, S.; Roubeau, O.; Teat, S. J.; Gamez, P. *Inorg. Chem.* **2014**, *53*, 9827−9836. (b) Yan, Z.; Li, J.-Y.; Liu, T.; Ni, Z.-P.; Chen, Y.-C.; Guo, F.-S.; Tong, M.-L. *Inorg. Chem.* **2014**, *53*, 8129−8135. (c) Wannarit, N.; Roubeau, O.; Youngme, S.; Teat, S. J.; Gamez, P. *Dalton Trans.* **2013**, *42*, 7120−7130. (d) Arcis-Castillo, Z.; Pineiro-Lopez, L.; Muñoz, M. C.; Ballesteros, R.; Abarca, B.; Real, J. A. *CrystEngComm* **2013**, *15*, 3455−3462. (e) Sorai, M.; Yumoto, Y.; Dost, M. H.; Larkworthy, L. F. *J. Phys. Chem. Solids* **1993**, *54* (4), 421−430.
(26) Nakamoto, T.; Tan, Z.-C.; Sorai, M. *Inorg. Chem.* **2001**, *40*, 3805−3809.

DOI: 10.1021/ic503040f
Inorg. Chem. 2015, 54, 2902−2909

NOTE ADDED AFTER ASAP PUBLICATION

This paper was published on the Web on March 2, 2015, with a minor error in the caption of Figure 2. The corrected version was reposted on March 3, 2015.

DOI: 10.1021/ic503040f
Inorg. Chem. 2015, 54, 2902−2909